

An Experimental $TE_{12} - TE_{11}$ Circular Waveguide Mode Converter

D. Hoppe

Radio Frequency and Microwave Subsystems Section

This article describes theoretical and experimental results for a prototype $TE_{12} - TE_{11}$ circular waveguide mode converter. The system which requires such a device, the high power Ka-Band transmitter is described briefly. A short review of coupled mode theory is given, and the theoretical performance of the final converter design is given. Experimental results for the fabricated converter are presented and compared with theory. A method of identifying the various circular waveguide modes in a multimode device is described. Given the close agreement between the theoretical predictions and experimental results, the computer code may be used with confidence in the design of future multimode tapers and mode converters.

I. Introduction

Previous reports have described the conceptual design of a high power Ka-Band transmitter (Ref. 1), theoretical calculations of mode purity effects on the performance of the system (Ref. 2), and the feed which will be used with the Ka-Band transmitter and transmission line (Ref. 3). This article focuses on another component in the system, the $TE_{12} - TE_{11}$ mode converter.

Conventional klystrons are not capable of producing 400 kW CW at 34.5 GHz, which is the required power level and frequency for the Ka-Band transmitter. The problem arises since, as the klystron output cavity is scaled to higher frequencies, its dimensions are decreased. It soon becomes impossible to extract 400 kW CW from the beam in the reduced interaction volume without exceeding a power density of 1 kW/cm² on the cavity walls. The power density of 1 kW/cm² represents an approximate upper limit which is set by the present state of the art in cooling technology.

In order to increase the interaction volume, an unconventional microwave tube, the gyroklystron, will be used. Two possible configurations for such a device are shown in Fig. 1. In both cases several circular waveguide cavities operating in the dominant TE_{11} circular waveguide mode prebunch the beam. The energy is extracted in the output cavity, which is an open-ended resonator that resonates in the higher order TE_{12} circular waveguide mode. This allows the output cavity dimensions to be increased thus allowing 400 kW to be extracted from the beam without exceeding 1 kW/cm² on the cavity walls. The microwave energy then exits the output cavity in a rotating TE_{12} circular waveguide mode.

Unfortunately the TE_{11} mode, not the TE_{12} mode, is the most suitable mode to use in the rest of the system. The TE_{12} mode has a radiation pattern which is totally unsuitable for illuminating the subreflector. The pattern is multilobed with the main radiation appearing off the waveguide axis. The TE_{11} mode on the other hand has the conventional dominant-mode pattern which is easily modified by the feed to give the

optimum Gaussian pattern for illuminating the shaped sub-reflector. For these reasons it is necessary to develop a device which will convert the TE_{12} mode to the TE_{11} mode. Two different locations for the converter are possible, one inside the vacuum envelope of the tube (Fig. 1[a]), and the other in the 1.75-in. transmission line (Fig. 1[b]). This article describes experimental and theoretical results for a small diameter device suitable for the in-tube configuration depicted in Fig. 1[a].

II. Mode Converter Theory

When the diameter of a circular waveguide exceeds $0.766 \lambda_0$ at the frequency of operation, the microwave signal may propagate in more than one circular waveguide mode. For a perfectly straight circular waveguide, these modes are orthogonal and no energy is exchanged between them. When the guide deviates from perfection, either by design or by accident, mode conversion occurs, and the modes become coupled.

The general deformed waveguide may be specified by writing the radius as a function of z , and ϕ as follows (Ref. 4, and J. Doane, "Propagation and mode coupling in corrugated and smooth wall circular waveguide," Plasma Physics Laboratory (internal document), Princeton, New Jersey):

$$r(z, \phi) = r_0 + \sum_{\ell} \alpha_{\ell}(z) \cos \ell\phi + \sum_k \alpha_k(z) \sin k\phi \quad (1)$$

In general, the azimuthal order of the perturbation (ℓ and k) determines which modes will be coupled. For example, a pure $\ell = 1$ perturbation causes coupling between the TE_{ij} , TM_{ij} mode group and the $TE_{(i\pm 1)m}$ and $TM_{(i\pm 1)m}$ mode groups. The $\ell = 1$ perturbation corresponds to curvature. Therefore an incident TE_{11} mode is coupled to the TE_{0m} , TM_{0m} , TE_{2m} and TM_{2m} modes through the curvature. Similarly a radial perturbation with no azimuthal variation, $\ell = 0$, and only a longitudinal variation, couples modes with the same azimuthal index. This is the type of coupling that occurs in circular waveguide tapers and horns.

The first step in a mode converter design is to determine what order of azimuthal variation is required. For example, a $TE_{ij} - TE_{mn}$ converter requires a perturbation of order ℓ where $\ell = |m - i|$. For modes of the same first index a circularly symmetric ($\ell = 0$) perturbation is required, for modes differing by 1 in first index a curvature ($\ell = 1$) perturbation is needed, modes differing by 2 require an elliptical deformation, and so on.

When the $\ell = |m - i|$ perturbation is chosen the incident TE_{ij} mode is coupled to all the $TE_{(i\pm\ell)p}$ and $TM_{(i\pm\ell)p}$ modes. In order to enhance the coupling to only the desired $TE_{(i\pm\ell)n}$ mode the perturbation is repeated at a specific interval in z , which is approximately given by the beat wavelength between the two modes of interest. The beat wavelength between modes 1 and 2, $\lambda_{1,2}$ is given by

$$\lambda_{1,2} = \frac{\lambda_1 \lambda_2}{|\lambda_1 - \lambda_2|} \quad (2)$$

In summary the rough design of the $TE_{ij} - TE_{mn}$ converter consists of a $\ell = |i - m|$ radial perturbation repeated longitudinally at an interval given by Eq. (2) where mode 1 is the TE_{ij} mode, and mode 2 is the TE_{mn} mode.

In order to accurately determine the number of perturbations required, their magnitude, and their exact placement, a detailed analysis of the coupled mode problem must be undertaken. The propagation in an arbitrarily deformed circular waveguide can be described by the following matrix equation:

$$\frac{d\mathbf{A}(z)}{dz} = -j [\beta(z)] \mathbf{A}(z) + [C(z)] \mathbf{A}(z) \quad (3)$$

Here

$\mathbf{A}(z)$ = a vector containing the mode amplitudes

$[\beta(z)]$ = a diagonal matrix containing the propagation coefficients

$[C(z)]$ = a matrix containing the coupling coefficients for the local waveguide perturbation.

Each term of $[C(z)]$, C_{ij} , is determined by the azimuthal order of the local perturbation, its magnitude, and the specific modes i and j (Ref. 4, and J. Doane, "Propagation and mode coupling in corrugated and smooth wall circular waveguide," Plasma Physics Laboratory (internal document), Princeton, New Jersey). The propagation of coefficient β_{ij} is determined for each mode by using the local radius.

A computer program was developed to solve Eq. (3) for the special case of arbitrary radial perturbations with no azimuthal variation $r(z, \phi) = r(z)$, and modes with first index 1. This is sufficient for the specific mode converter design required, $TE_{12} - TE_{11}$, i.e., $\ell = 0$.

Following the method outlined by Moeller (Ref. 5) the radial perturbation was taken to be sinusoidal with respect to z ,

$$r(z) = r_0 + \Delta r \cos\left(\frac{2\pi z}{\lambda_B}\right) \quad (4)$$

The average radius was chosen to be 0.423 inches which is slightly larger than the radius of the tube's output cavity. The number of ripples was chosen to be seven, and in order to obtain maximum conversion efficiency at the design frequency of 34.5 GHz optimum values of 0.039 inches and 1.364 inches were found for Δr and λ_B respectively. These values were optimized by solving Eq. (3) for various combinations of Δr and λ_B . Seven ripples were chosen since the theoretical ripple magnitude required for the seven ripple device was small enough that no modes become trapped in the ripples at the design frequency of 34.5 GHz. This condition is required for accurate modeling of the interaction with the existing computer code. A cross sectional view of the final device is shown in Fig. 2.

The mode converter is a reciprocal device. That is, an input TE_{12} mode will be converted to an output TE_{11} mode with exactly the same efficiency as an input TE_{11} mode is converted into a TE_{12} mode. Although the final device will be used as a $TE_{12} - TE_{11}$ converter it is simplest to test it reciprocally as a $TE_{11} - TE_{12}$ mode converter. Figure 3 shows the mode composition as a function of z when a TE_{11} mode is incident on the device. In this plot, and throughout the remainder of this paper, dBc denotes the amount of power carried by any waveguide mode with respect to the input TE_{11} mode power. The theoretical final output mode composition is summarized in the last column of Table 1. The efficiency of the conversion is found to be 99.77%. The device efficiency when it is operating in the reciprocal mode will also be 99.77% but the spurious output power will be contained in other modes. The conversion efficiency is plotted as a function of frequency in Fig. 4. The computer program was also used to determine the allowable tolerances on r_0 , Δr , and λ_B to be given to the machine shop in order to ensure high conversion efficiency for the fabricated device. The most sensitive of the parameters was found to be the average radius, r_0 , which must be held to ± 0.001 inches to maintain 99% efficiency. An error of about ± 0.002 inches was found to be acceptable for the ripple magnitude, Δr , while significant errors in the ripple period, λ_B , were permissible.

III. Experimental Results

The device depicted in Fig. 2 was fabricated in 3 sections, one section of 3 ripples, and two containing two ripples each.

In addition to making the fabrication easier, dividing the device up in this manner also allows experimental measurement of the mode content after 2, 3, 4 and 5, as well as the total number of ripples, 7. Two additional tapers were fabricated, one from the existing rectangular to circular waveguide transition output radius of 0.184 inches to the converter input radius of 0.462 inches, and one from the converter output radius of 0.462 inches to the proposed transmission line radius of 0.875 inches.

As we discussed earlier the mode converter is tested reciprocally as a $TE_{11} - TE_{12}$ mode converter. A block diagram of the experimental set-up used on the antenna range is shown in Fig. 5. A circular waveguide taper connects the rectangular to circular transition output diameter to the input diameter of the converter. The TE_{11} mode undergoes some mode conversion in this taper, and the TE_{11} plus the spurious TE_{1n} and TM_{1n} modes then enter the rippled sections. The mode most strongly coupled in this taper, the TM_{11} mode, was measured to be at level of approximately 22.0 dB below the TE_{11} power at the first taper output. The method of determining mode content via pattern measurement is discussed in Appendix A. This slightly impure signal then passes through the mode converter, and through an up taper (which also causes a slight amount of additional mode conversion) to the final diameter of 1.75 inches. By inserting a variable number of rippled sections between the two tapers, and measuring the far field pattern of the taper-ripple-taper chain, the mode content after 0, 2, 3, 4, 5 and 7 ripples was determined.

The patterns measured when no sections are inserted between the two tapers are shown in Fig. 6, along with the ideal TE_{11} patterns which would be measured if there were no mode conversion in the two tapers. Figure 7 shows the measured patterns when the entire converter (7 sections) is inserted between the tapers. The theoretical TE_{12} patterns, which would be measured if the tapers caused no mode conversion and the mode converter were perfect, are also plotted in Fig. 7. The intermediate patterns measured when 3 sections were inserted between the tapers are shown in Fig. 8. Measurements were also taken for 2, 4 and 5 ripple configurations, at the design frequency of 34.5 GHz.

By using the methods described in Appendix A, the mode composition at the output of the final taper was estimated for each of the configurations mentioned above. In particular, estimates for the 0, 3, and 7 ripple cases are summarized in Table 1. The estimated mode content from the measurements is also plotted on Fig. 3 for comparison with theory.

A final set of measurements was made to experimentally determine the conversion efficiency vs. frequency characteristics of the mode converter. For these measurements the

total converter was inserted between the tapers, and pattern measurements were taken for frequencies of 34.0, 34.2, 34.4, 34.5, 34.6, and 34.8 GHz. The mode composition was then determined and the results for the measured efficiency vs. frequency are plotted in Fig. 4 for comparison with theory.

IV. Discussion

In comparing the experimental and theoretical results for the patterns of the tapers connected together with no rippled sections between them, we see that excellent agreement is found between the theoretical TE_{11} H plane pattern and the measured H -plane pattern. The agreement in the E plane is not as good. This is expected since the taper system produces spurious TM_{11} and TM_{12} modes whose effects are only seen in the E plane. Figure 8 again shows good agreement in both planes, with more error in the E plane. This can be explained by considering the taper effects again. The short 0.368–0.924 inch taper generates some spurious TM_{11} power which enters the mode converter. Computer simulations show that spurious TM_{11} power entering the device will be converted primarily into TM modes at the output of the device. Once again, the effects of these modes are only visible in the E plane. The slight asymmetries which are detectable in the measured patterns are probably due to slight misalignments between the taper and mode converter sections.

When the theoretical mode content along the converter and that derived by pattern measurement after 0, 2, 3, 4, 5 and 7 ripples are compared in Fig. 3, excellent agreement is found for the TE_{11} and TE_{12} modes. However, poor agreement is found for the TM_{11} and TM_{12} modes. As was mentioned earlier a spurious TM_{11} signal at a level of approximately –22 dBc was found at the output of the first taper. This signal then enters the rippled sections where it is converted primarily into TM modes. These spurious effects overwhelm the calculated TM_{11} and TM_{12} conversion effects for a pure TE_{11}

mode input, but have little effect on the dominant TE_{11} – TE_{12} interaction. This explains the good agreement seen for the TE_{11} and TE_{12} modes and poor agreement for the TM modes. Despite the spurious effects an overall efficiency over 99.5% was measured for the device (See Table 1), which is also in good agreement with the calculated value of 99.77%.

For the bandwidth results shown in Fig. 4 the best agreement between theory and measurement is found for the points within 100 MHz of the design frequency. For frequencies further removed from 34.5 GHz some of the disagreement may be attributed to errors in the theoretical calculations. For all frequencies, four forward traveling modes were used to model the interaction in the ripples. For the higher frequencies shown in the figure this is probably not sufficient since the TE_{13} mode may also propagate. For the lower frequencies the TM_{12} mode becomes trapped in between the ripples, and reflected waves which are not included in the computer model become important.

V. Conclusions

In conclusion, theoretical and experimental results for a prototype TE_{12} – TE_{11} mode converter have been presented. Good agreement between theory and experiment was found in most cases, and reasonable explanations have been given for the instances where some disagreement has been found. The computer code used to generate the theoretical results presented in this report may now be used with confidence in the design of multimode tapers, mode converters and other devices. The pattern measurement technique for mode identification has also been proved, and may be used to characterize other components. Future work will include an upgrade of the computer code allowing the inclusion of reflected modes. This places confidence in the design of a possible future mode converter which may be placed in the 1.75 inch diameter transmission line for use with a system configured as shown in Fig. 1[b].

Acknowledgments

The author would like to thank H. Reilly who supervised the fabrication of the tapers and mode converter sections, and S. Stride who assisted in the far field pattern measurements.

References

1. Bhanji, A., Hoppe, D., Hartop, R., Stone, E., Imbriale, W., Stone, D., and Caplan, M., High power Ka-band transmitter for planetary radar and spacecraft uplink, *TDA Progress Report 42-78* (April-June 1984), Jet Propulsion Laboratory, Pasadena, CA, pp. 24-48.
2. Hoppe, D., Imbriale, W., and Bhanji, A. The effects of mode impurity on Ka-band system performance, *TDA Progress Report 42-80* (Oct.-Dec. 1984), Jet Propulsion Laboratory, Pasadena, CA, pp. 12-23.
3. Hoppe, D., Propagation and radiation characteristics of a multimode corrugated waveguide feedhorn, *TDA Progress Report 42-82*, Jet Propulsion Laboratory, Pasadena, CA.
4. Levine, J., Rippled wall mode converters for circular waveguide, *International Journal of Infrared and Millimeter Waves*, Vol. 5, No. 7, pp. 937-952, 1984.
5. Moeller, C., Mode converters used in doublet III ECH microwave system, *Int. J. Elect.*, Vol. 53, No. 6, pp. 573-585, 1982.

Table 1. Measured TE_{11} - TE_{12} mode converter performance. Mode composition after N mode converter sections.

Mode	Measured			Theory
	$N = 0$	$N = 3$	$N = 7$	$N = 7$
$TE_{11}, \%$	98.23	59.09	*	0.005
$TM_{11}, \%$	1.66	2.45	0.19	0.17
$TE_{12}, \%$	*	37.99	99.57	99.77
$TM_{12}, \%$	0.0025	0.48	0.21	0.05
Others, %	*	*	0.025	0

* No power measured down to system sensitivity.

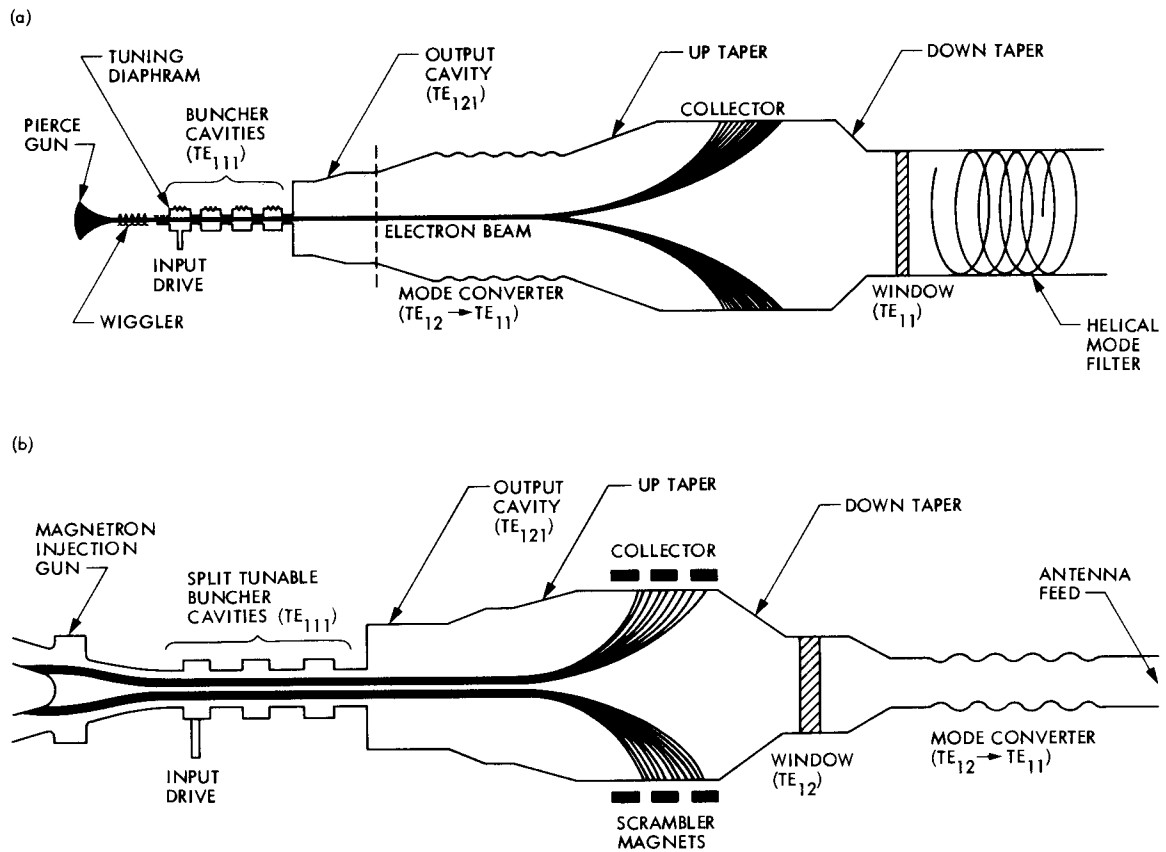


Fig. 1. Two possible gyrokystron configurations: (a) phase 1, (b) phase 2

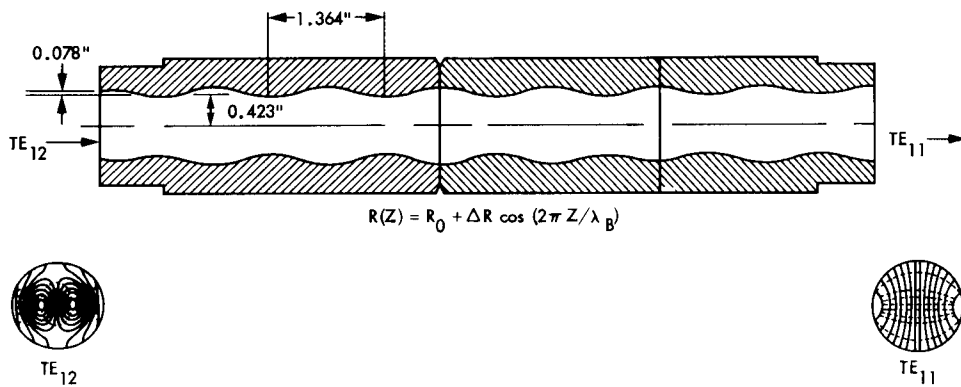


Fig. 2. TE_{12} - TE_{11} mode converter

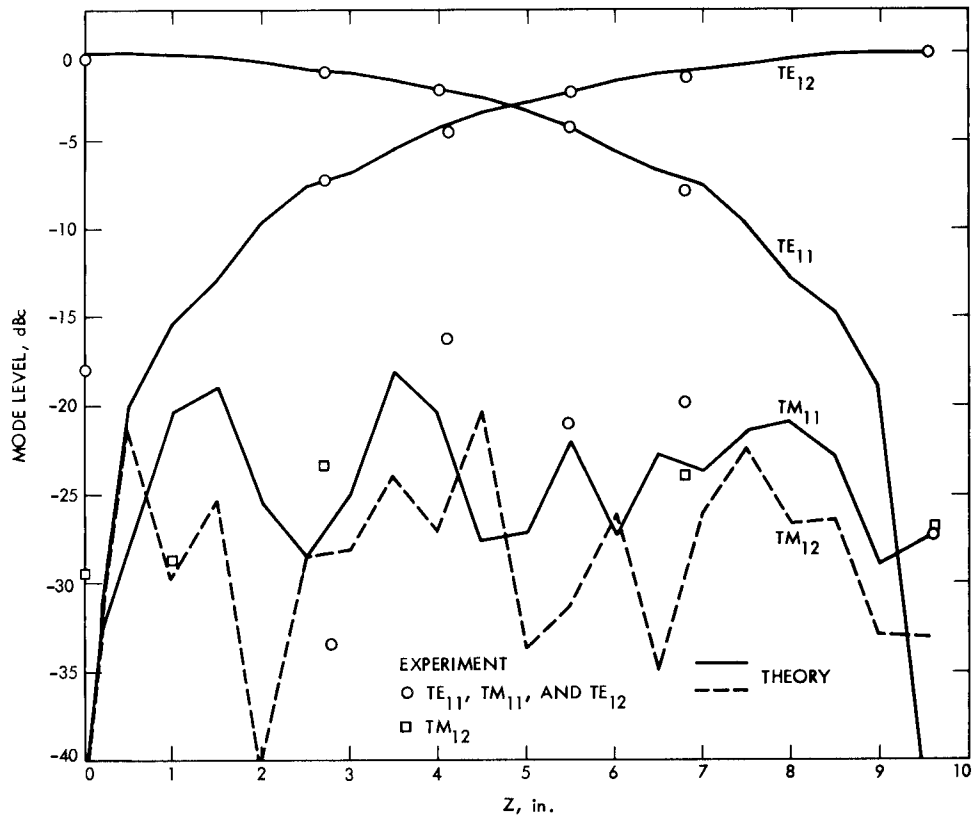


Fig. 3. Mode composition as a function of longitudinal coordinate for the $TE_{11}-TE_{12}$ mode converter

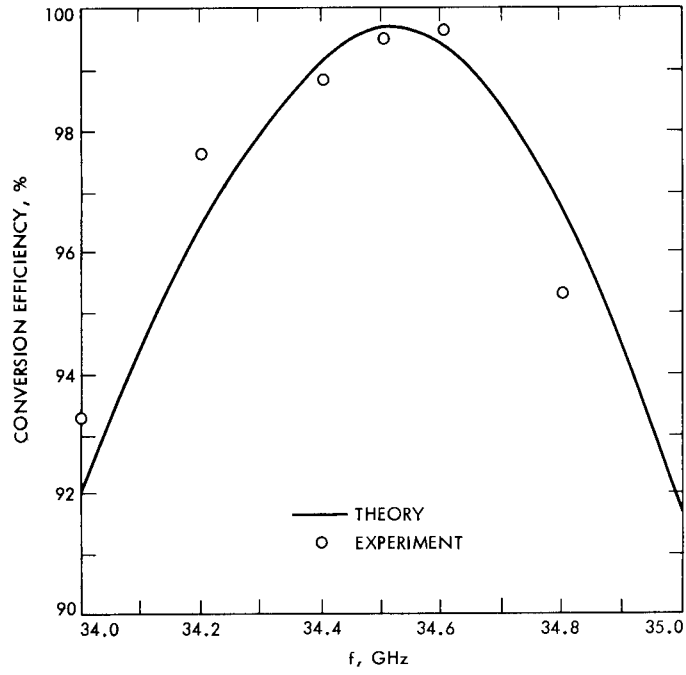


Fig. 4. TE_{11} - TE_{12} mode conversion efficiency vs frequency

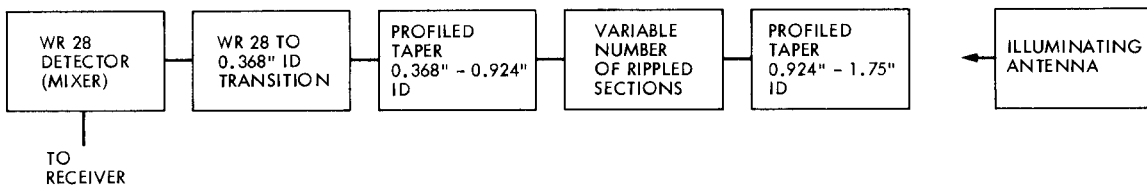


Fig. 5. Antenna range test set up

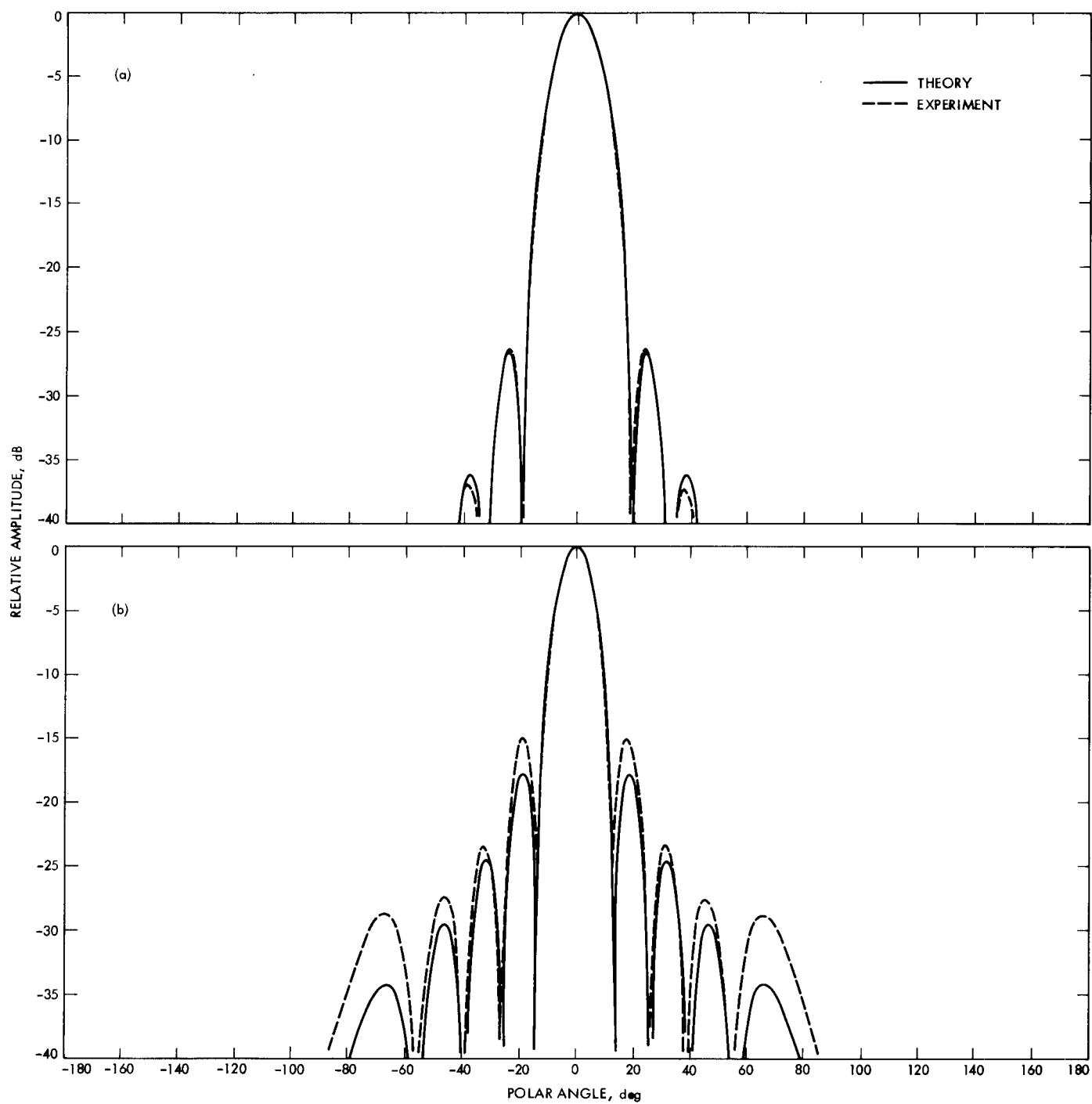


Fig. 6. Taper radiation patterns: (a) H plane patterns, (b) E plane patterns

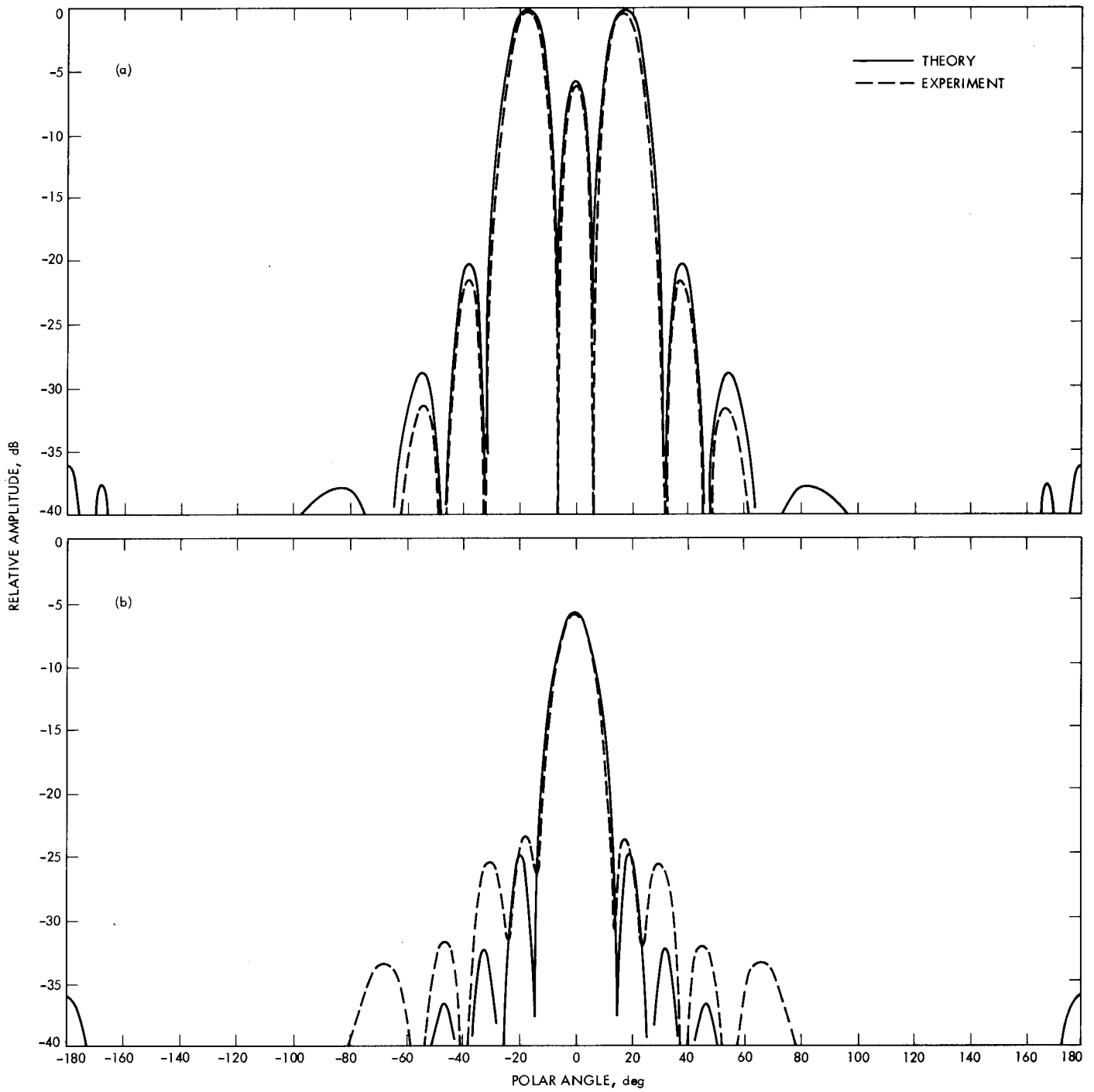


Fig. 7. Total mode converter radiation patterns: (a) H plane patterns, (b) E plane patterns

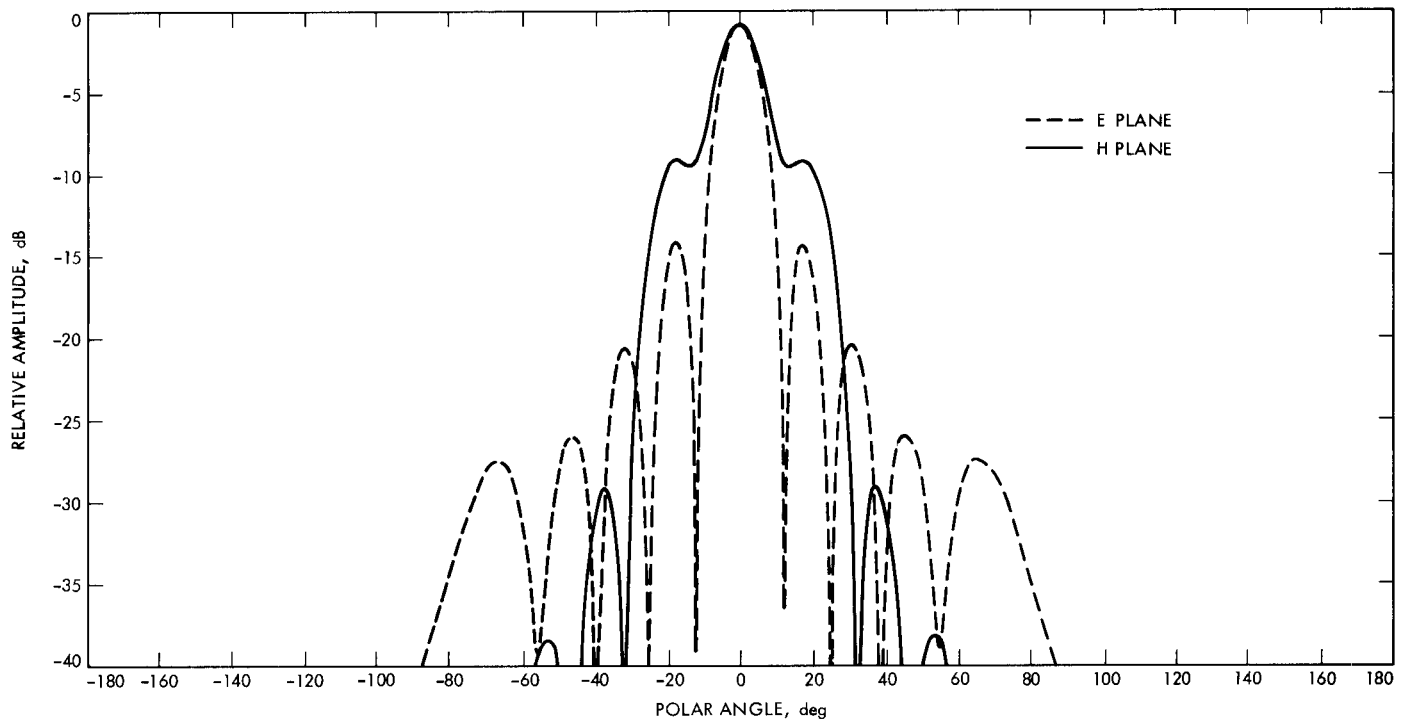


Fig. 8. Three ripple mode converter. Measured radiation patterns.

Appendix A

Mode Identification Using Far Field Radiation Pattern Measurements

In this appendix a method of mode identification in a multimode circular waveguide is explained briefly.¹ The far field radiation pattern for an arbitrary combination of circular waveguide modes assuming small reflection from the aperture is given by (Refs. A-1, A-2):

$$\begin{aligned}
 E(R, \theta, \phi) = & \frac{k \exp(-jkR) (1 + \cos \theta)}{2R} a^2 \\
 & \times \sum_{m,n}^{M,N} \left[\left(C_{mn} (P_{mn})^{1/2} \exp(j\phi_{mn}) \frac{J_m(ka \sin \theta)}{ka \sin \theta} \right. \right. \\
 & \left. \left. - \tilde{C}_{mn} (\tilde{P}_{mn})^{1/2} \exp(j\tilde{\phi}_{mn}) ka \sin \theta \frac{J_m(ka \sin \theta)}{X_{mn}^2 - (ka \sin \theta)^2} \right) \sin m \phi a_\theta \right. \\
 & \left. \times C_{mn} (P_{mn})^{1/2} \exp(j\phi_{mn}) \frac{J'_m(ka \sin \theta)}{(X'_{mn})^2 - (ka \sin \theta)^2} \cos m \theta a_\phi \right]
 \end{aligned} \tag{A-1}$$

where

$$k = 2\pi/\lambda_0$$

$$\lambda_0 = \text{Wavelength}$$

$$R = \text{Far field radius}$$

$$a = \text{Waveguide radius}$$

$$P_{mn} = \text{Power carried by the } TE_{mn} \text{ mode}$$

$$\tilde{P}_{mn} = \text{Power carried by the } TM_{mn} \text{ mode}$$

$$\phi_{mn} = \text{Phase of the } TE_{mn} \text{ mode}$$

$$\tilde{\phi}_{mn} = \text{Phase of the } TM_{mn} \text{ mode}$$

$$C_{mn} = \text{Normalization constant for the } TE_{mn} \text{ mode}$$

$$\tilde{C}_{mn} = \text{Normalization constant for the } TM_{mn} \text{ mode}$$

$$X_{mn} = \text{Zero of } J_m(X)$$

$$X'_{mn} = \text{Zero of } J'_m(X)$$

M, N = Indices chosen large enough to include all propagating modes in the waveguide.

Equation (A-1) assumes that only one of the two orthogonally polarized sets of modes, the set where $E_r \propto \sin \phi$, exists in the waveguide. If we further assume only modes with one azimuthal variation exist, $m = 1$, as in the $TE_{12} - TE_{11}$ mode converter, or tapers, we may write the following equations for the form of the radiation in the E and H planes, respectively, as

E plane

$$\begin{aligned}
 E \propto \sum_{n=1}^N \left(C_{1n} (P_{1n})^{1/2} \exp(j\phi_{1n}) \frac{J_1(ka \sin \theta)}{ka \sin \theta} \right. \\
 \left. - \tilde{C}_{1n} (\tilde{P}_{1n})^{1/2} \exp(j\tilde{\phi}_{1n}) \frac{ka \sin \theta J_1(ka \sin \theta)}{X_{1n}^2 - (ka \sin \theta)^2} \right)
 \end{aligned} \tag{A-2}$$

H plane

$$E \propto \sum_{n=1}^N C_{1n} (P_{1n})^{1/2} \exp(j\phi_{1n}) \frac{J'_1(ka \sin \theta)}{(X'_{1n})^2 - (ka \sin \theta)^2} \tag{A-3}$$

From Eq. (A-3) we see that only TE modes contribute to the radiation in the H plane. Furthermore, if we examine the radiation in this plane at the point $ka \sin \theta = X'_{1p}$, where $J'_1(X'_{1p}) = 0$, it is found that all TE_{1n} modes have a null at this point, except the mode TE_{1p} where the denominator and numerator in Eq. (A-3) vanish. Thus, by examining the H plane pattern at the points $ka \sin \theta = X'_{1n}$, $n = 1, \dots, N$ the relative levels of all the TE_{1n} modes may be determined, in terms of power, since the normalization constants C_{1n} are known.

Similarly the relative levels of the TM_{1n} modes may be determined by examining the E plane pattern at the points where $ka \sin \theta = X_{1n}$. In this manner all of the TE_{1n} , and TM_{1n} modes may be identified. The method may be extended to include the orthogonal set of $m = 1$ modes by including polarization considerations, and the modes with other azimuthal variation, $m = 0, 2, 3, \dots$ may be identified by taking more pattern cuts.²

¹A more detailed discussion can be found in Z. Zhang, M. Thumm, and R. Wilhelm, "Far field radiation patterns from open-ended oversized circular waveguides and identification of multimode outputs of gyrotrons," Institute für Plasma für schung, Universität Stuttgart (internal document).

²Z. Zhang, M. Thumm, and R. Wilhelm, *op. cit.*

References

- A-1. Silver, S., *Microwave Antenna Theory and Design*, Rad. Lab. Ser., Vol. 12. New York: McGraw-Hill, pp. 336–338, 1949.
- A-2. Ludwig, A. C., Radiation pattern synthesis for circular aperature horn antennas, *IEEE Trans. Antennas and Propagation*, Vol. AP-14, pp. 434–440., July 1966.